# Correlation for the Viscosity of Sulfur Hexafluoride ($SF_6$) from the Triple Point to 1000 K and Pressures to 50 MPa

Cite as: J. Phys. Chem. Ref. Data **41**, 023102 (2012); https://doi.org/10.1063/1.3702441
Submitted: 11 January 2012 . Accepted: 22 March 2012 . Published Online: 23 April 2012

Sergio E. Quiñones-Cisneros, Marcia L. Huber, and Ulrich K. Deiters

# Correlation for the Viscosity of Sulfur Hexafluoride ($SF_6$) from the Triple Point to 1000 K and Pressures to 50 MPa

**Sergio E. Quiñones-Cisneros**[a)]
*Instituto de Investigaciones en Materiales, Universidad Nacional Autónoma de México, Apdo. Postal 70-360, México D.F. 04510, México*

**Marcia L. Huber**
*Thermophysical Properties Division, National Institute of Standards and Technology, 325 Broadway, MS 638.08, Boulder, Colorado 80305-3337, USA*

**Ulrich K. Deiters**
*Institute of Physical Chemistry, University of Cologne, Luxemburger Str. 116, 50939 Cologne, Germany*

(Received 11 January 2012; accepted 22 March 2012; published online 23 April 2012)

A wide-ranging correlation for the viscosity surface of sulfur hexafluoride ($SF_6$) has been developed that incorporates generalized friction theory (GFT). The approach requires, as the core thermodynamic model, a reference-quality equation of state (EoS). Here the EoS of Guder and Wagner has been selected for that purpose. All available experimental data, to the extent of our knowledge, were considered in the development of the model. The correlation performs best in the low-pressure (less than 0.33 MPa) region from 300 K to 700 K where the estimated uncertainty (considered to be combined expanded uncertainty with a coverage factor of two) is 0.3%. In the region from 300 K to 425 K for pressures less than 20 MPa, the estimated uncertainty is less than 1%. Where there were data available for validation at temperatures from 230 K to 575 K for pressures up to 50 MPa, the estimated uncertainty is 2%. The correlation extrapolates in a physically reasonable manner and may be used at pressures to 100 MPa and temperatures from the triple point to 1000 K.  [http://dx.doi.org/10.1063/1.3702441]

Key words: generalized friction theory; sulfur hexafluoride; viscosity.

## CONTENTS

1. Introduction . . . . . 2
2. Model Formulation . . . . . 3
   2.1. Dilute-gas limit . . . . . 4
   2.2. Initial density dependence . . . . . 5
   2.3. Residual friction model . . . . . 5
3. Regression and Results . . . . . 6
   3.1. Low-density results . . . . . 8
   3.2. Full-range results . . . . . 8
4. Computer-Program Verification . . . . . 10
5. Conclusion . . . . . 10
   Acknowledgements . . . . . 10
6. References . . . . . 10

### List of Tables

1. Summary of available experimental data. Considered sets: primary (1), secondary (2), and tertiary (3) . . . . . 3
2. Dilute-gas model parameters for $SF_6$ . . . . . 4
3. Parameters for the second viscosity virial coefficient . . . . . 5
4. Residual friction model parameters for sulfur hexafluoride . . . . . 6
5. Primary data friction theory model results . . . . . 7
6. Secondary data friction theory model results . . . 7
7. Tertiary data friction theory model results . . . . . 8
8. Sample points for computer verification of the model . . . . . 10

### List of Figures

1. $SF_6$ dilute-gas model (solid line) along with low-density primary data . . . . . 4
2. $SF_6$ dilute-gas model (solid line) along with low-density secondary and other data . . . . . 4
3. Comparison of zero-density and atmospheric-pressure correlations in the literature . . . . . 5
4. Second viscosity virial coefficient $B_\eta$ . . . . . 5
5. $SF_6$ model $\eta$-$T$ surface performance near the phase boundary . . . . . 6

[a)]Author to whom correspondence should be addressed; Electronic mail: seqc@mac.com.

6. Overall $SF_6$ model $\eta$-$T$ surface performance ..... 6
7. Separation of the pressure into attractive and repulsive parts based on the internal pressure Eqs. (2) and (3) for the $SF_6$ reference EoS of Guder (Ref. 8) ..... 7
8. Deviation-$p$-$T$ diagram ..... 8
9. Low-density primary data model deviation .... 8
10. Low-density secondary data model deviations ..... 9
11. Full density range primary data model deviations ..... 9
12. Full pressure range primary data model deviations ..... 9
13. Full temperature range primary data model deviations ..... 9
14. Full density range secondary data model deviations ..... 9
15. Full pressure range secondary data model deviations ..... 9
16. Overall deviation performance of all data considered in the regression..... 10

## 1. Introduction

Because of its chemical inertia and the almost spherical shape of its molecules, sulfur hexafluoride ($SF_6$) has sometimes been called a synthetic noble gas. It has many technical applications, such as an insulator for high-voltage equipment,[1] thermoacoustic insulation of windows, and a newer application as an inert solvent for chemical reactions in supercritical fluids.[2] In addition, there are medical applications of $SF_6$ (Refs. 3 and 4) and it also is of interest to researchers involved with molecular simulations.[5–7] At temperatures above 1000 K, decomposition can occur, and $SF_6$ begins to attack metal or silica surfaces. This leads to other technical applications such as surface fluorination or etching, but makes it difficult to obtain experimental data for pure $SF_6$ at these temperatures.

As $SF_6$ is an important industrial fluid, it is necessary to have accurate models for its thermophysical properties. Guder and Wagner[8] reviewed the thermodynamic properties of $SF_6$ and developed a reference equation of state. Assael *et al.*[9] recently developed a reference correlation for the thermal conductivity surface of $SF_6$. At present, as noted by Wilhelm *et al.*,[10] a suitable reference viscosity surface is not available. Wilhelm *et al.*[10] pointed out that the surface correlation presented by Altunin[11] was primarily based on only three data sets (Ulybin and Makarushkin,[12] Timrot *et al.*,[13] and Grigorev *et al.*[14]), and the resulting correlation fails to represent the data of Hoogland *et al.*,[15] as well as their own data. Similarly, the surface of Hafer[16,17] also fails to adequately represent the data of Hoogland *et al.*[15] In addition, both of these surfaces were developed prior to the availability of the extensive data provided by Wilhelm *et al.*[10] In this work, we take advantage of the availability of the new data of Wilhelm *et al.*[10] to develop a wide-ranging viscosity correlation and provide comparisons to literature data and other correlations. The formulation is based on the generalized friction theory (GFT) method[18] that can provide an accurate description of the viscosity surface, including the liquid, vapor and supercritical regions.

Wilhelm *et al.*[10] surveyed the viscosity surfaces and data available to 2005, provided a critical evaluation of the available literature data, and we have incorporated their recommendations in this work. Table 1 summarizes, to the best of our knowledge, all available viscosity data for $SF_6$,[10,12–16,19–41] and includes the type of experimental apparatus, sample purity, author's estimated uncertainty, and the temperature and pressure ranges of the data. The data are identified as primary, secondary, or tertiary. The primary data were selected as those with the lowest uncertainties that cover a particular region; generally when there are overlapping regions, the sets with the larger uncertainties are considered secondary and are treated differently in the regression procedure described later in this document. Tertiary data were not used in the regression and were included only for comparison purposes. The primary set includes the extensive 2005 data of Wilhelm *et al.*[10] that were made with a vibrating wire apparatus in a relative mode with uncertainties ranging from 0.25% to 0.4% that extend to 20.4 MPa. The earlier quartz oscillating disk measurements from the Vogel group[37] also were considered as primary data; these cover temperatures from room temperature to 681 K and were performed at 0.33 MPa, with an uncertainty ranging from 0.1% to 0.3%, with the highest uncertainty at the highest temperatures. Comparisons with their work indicate that many of the early measurements[19,20,22,23] are several percent too high and these were considered tertiary. Although also subject to this problem, the set of Ellis and Raw[21] was included as secondary to guide the extrapolation behavior to high temperatures, since the data extend to 1126 K. Several data sets from Kestin and coworkers[25,28–31] that extend above room temperature are thought to have a temperature measurement error, as discussed by Vogel *et al.*,[42] and were not included as primary data. The 1971 Kestin[43] data set at 298 K, however, agrees with the results of Strehlow and Vogel[37] to within 0.2% and was included in the primary set. The high-pressure region was supplemented with the secondary data set of Ulybin and Makarushkin[12] that extends to 51 MPa. Following the recommendations in Wilhelm *et al.*,[10] we also include as primary data the capillary measurements of Hoogland *et al.* that were performed in an absolute mode[15] and the measurements by Hurly *et al.*[38] at 298 K made in a Greenspan viscometer. Although a discussion detailing the apparatus has been published,[17] the large experimental data set in the thesis of Hafer[16] is not yet published in the literature and was considered as tertiary data. All data from this work, obtained from both forced-mode and free-mode measurements from a torsional crystal viscometer, are included in Table 1; however, Hafer used only the forced-mode data in the development of his correlation. Since the work of Wilhelm *et al.*,[10] only two additional small data sets have been published: the

TABLE 1. Summary of available experimental data. Considered sets: primary (1), secondary (2), and tertiary (3)

| 1st author | Year | Method[a] | Purity, % | Unc., % | No. points | $T$ (K) | $p$ (MPa) | Sets |
|---|---|---|---|---|---|---|---|---|
| Earwicker[19] | 1954 | CAP | n/a | n/a | 2 | 295–373 | 0.1 | 3 |
| McCoubrey[20] | 1957 | CAP | n/a | 1 | 8 | 295–478 | 0.1 | 3 |
| Ellis[21] | 1959 | CAP | 99 | 1 | 17 | 470–1126 | 0.1 | 2 |
| Raw[22] | 1963 | CAP | 95 | 1 | 4 | 303–342 | 0.0016 | 3 |
| Dawe[23] | 1970 | CAP | 99.9 | 1 | 20 | 293–873 | 0.1 | 3 |
| Kestin[24] | 1971 | OD | 99.99 | 0.10 | 2 | 296–303 | 0.1 | 1 |
| Hellemans[25] | 1973 | OD | 99.99 | 0.1–0.3 | 7 | 298–573 | 0.1 | 3 |
| Ueda[26] | 1974 | OD | n/a | n/a | 8 | 273–346 | 0.07 | 2 |
| Timrot[13,27] | 1975 | OD | 99.8 | 0.7 | 62 | 297–526 | 0.04–3.46 | 2 |
| Kestin[28] | 1976 | OD | 99.99 | 0.2 | 3 | 296–477 | 0.1 | 3 |
| Kestin[29] | 1977 | OD | 99.99 | 0.1–0.2 | 10 | 296–474 | 0.1 | 3 |
| Kestin[30] | 1977 | OD | 99.99 | 0.1–0.2 | 5 | 298–473 | 0.1 | 3 |
| Grigorev[14] | 1977 | CAP | 99.78 | 0.7–1.1 | 131 | 245–473 | 2–40 | 2 |
| Ulybin[12] | 1977 | CAP | 99.8 | 1 | 89 | 230–300 | 0.3–51.2 | 2 |
| Abe[31] | 1979 | OD | 99.99 | 0.3 | 2 | 423–468 | 0.1 | 2 |
| Harris[32] | 1979 | CAP | 99.99 | 1.5 | 7 | 218–301 | 0.1 | 3 |
| Tanaka[33] | 1980 | RB | 99.5 | 1 | 12 | 298–348 | 0.1–0.2 | 3 |
| Hoogland[34] | 1982 | CAP | n/a | 0.2–1 | 13 | 318–323 | 3.7–4.1 | 2 |
| Lukin[35] | 1983 | CAP | n/a | 0.3 | 13 | 173–293 | 0.1 | 3 |
| Hoogland[15] | 1985 | CAP | n/a | 0.1 | 31 | 298–333 | 0.1–9.6 | 1 |
| Takahashi[36] | 1987 | OD | n/a | 0.5 | 34 | 273–319 | 1.2–3.7 | 2 |
| Strehlow[37] | 1989 | OD | 99.95 | 0.1–0.3 | 86 | 298–691 | 0.33 | 1 |
| Hafer[16,17] | 1999 | TOR | 99.996 | 3–6 | 2074 | 225–327 | 0.03–34.5 | 3 |
| Hurly[38] | 2003 | GRN | 99.99 | 0.5 | 15 | 298 | 0.3–1.6 | 1 |
| Wilhelm[10] | 2005 | VW | 99.995 | 0.25–0.4 | 677 | 300–425 | 0.03–20.4 | 1 |
| Berg[39,40] | 2005 | CAP | 99.99 | 0.04 | 1 | 298 | 0.1 | 1 |
| Estrada[41] | 2008 | GRN | 99.99 | 0.6 | 8 | 273 | 0.3–1 | 2 |

[a]CAP, capillary; GRN, Greenspan viscometer; OD, oscillating disk; RB, rolling ball; TOR, torsional crystal; VW, vibrating wire.

data of Berg[39,40] and those of Estrada-Alexanders and Hurly.[41] The single data point measured by Berg[39,40] in 2005 in a capillary flow instrument designed for high accuracy (0.04%) absolute viscosity in gases was also included in the primary data set. The data of Estrada-Alexanders and Hurly[41] were treated as secondary data, as they have slightly larger uncertainties. In this work, all temperatures have been converted to ITS-90 (Ref. 44) and all densities for the given state points are obtained from the equation of state (EoS) of Guder and Wagner[8] for the reported temperature and pressure. This may introduce additional uncertainty, because the densities we used may not be identical to the values used by the original researchers in their data analysis procedures.

## 2. Model Formulation

For the development of the reference viscosity model for $SF_6$, the GFT approach proposed by Quiñones-Cisneros and Deiters[18] has been applied. In general terms, a GFT model can be written as follows:

$$\eta = \eta_0 + \eta_f, \tag{1}$$

where $\eta_0$ corresponds to the dilute-gas limit and $\eta_f$ is a friction term. The $\eta_f$ is built upon a balance between repulsive and attractive contributions to the isotropic pressure. In the GFT approach, this is achieved by making use of the internal pressure ($\pi_T$) concept according to the following definitions:

$$p_a = -\pi_T, \tag{2}$$

and

$$p_r = p - p_a = T\left(\partial p \Big/ \partial T\right)_v. \tag{3}$$

In addition, as pointed out in the original GFT work,[18] for an accurate description of the low-density phase, an explicit separation of the linear ideal-gas term is recommended,

$$p_r = p_{id} + \Delta p_r. \tag{4}$$

The ideal-gas term provides the linear initial density-viscosity dependence responsible for the behavior of the second viscosity virial coefficient. The final full model that has been used is similar to the GFT model that was used for water and $CO_2$,[18]

$$\eta_f = \kappa_a p_a + \kappa_r \Delta p_r + \kappa_i p_{id} + \kappa_{aa} p_a^2 + \kappa_{rr} \Delta p_r^2 + \kappa_{ii} p_{id}^2 + \kappa_{rrr} p_r^3 + \kappa_{aaa} p_a^3, \tag{5}$$

where the $\kappa$ friction parameters depend only on temperature and an additional cubic term has been added in order to

achieve improved accuracy at high pressure. We note that, given the analytical nature of the EoS used for $SF_6$, the weak divergence of the viscosity in the near-critical region is not considered in this work. Nevertheless, as demonstrated by Quiñones-Cisneros and Deiters,[18] the use of a renormalized EoS may also reproduce the non-classical weak viscosity divergence, in close agreement with experimental microgravity measurements. Nevertheless, if required, the viscosity critical anomaly could also be addressed theoretically, as was done by Sengers *et al.* for water.[45]

### 2.1. Dilute-gas limit

For the dilute-gas limit, an empirical model as suggested for the GFT (Ref. 18) approach has been fitted to the primary low-density/low-pressure data (gas/vapor data up to 1 MPa). The model is of the form

$$\eta_0 = \left(d_0 + d_1 T_r^{1/4} + d_2 T_r^{1/2} + d_3 T_r^{3/4} + d_4 T_r\right), \qquad (6)$$

where $T_r = T/T_c$ is the reduced temperature, and the value for the critical temperature is consistent with the one used in the EoS of Guder and Wagner, $T_c = 318.7232$ K. The model fit is done by combining Eqs. (1), (5), and (6), but using only low-pressure data and eliminating the third-order terms in Eq. (5). The parameters for this dilute-gas correlation are given in Table 2. The primary data used in the regression were those of Kestin *et al.*,[43] Hoogland *et al.*,[15] Strehlow and Vogel,[37] Hurly *et al.*,[38] Berg,[39,40] and Wilhelm *et al.*[10] As secondary data, selected points from Ueda and Kigoshi,[26] Timrot *et al.*,[13] Abe *et al.*,[31] and Estrada-Alexanders and Hurly[41] were considered. Only low-pressure secondary points outside the temperature range covered by the primary data were used.

Figure 1 shows all primary low-pressure gaseous state data up to 0.5 MPa along with the derived dilute-gas empirical model. As illustrated in Fig. 1, all primary data fall closely over the model curve. The dilute-gas correlation is based on primary data that range from 270 K to 700 K, although Eq. (6) can be extrapolated with reasonable confidence from the triple point, 223.555 K,[46] up to 1000 K. Figure 2 shows a comparison with the secondary and all other low-pressure data available, giving some indication of the reliability of extrapolation outside the 270 K to 700 K range. The data in Fig. 2 are from Hafer,[16,17] Lukin *et al.*,[35] Tanaka *et al.*,[33] Harris *et al.*,[32] Ulybin and Makarushkin,[12]

TABLE 2. Dilute-gas model parameters for $SF_6$

| $i$ | $d_i$ (mPa s) |
|---|---|
| 0 | 0.118561 |
| 1 | −0.378103 |
| 2 | 0.416428 |
| 3 | −0.165295 |
| 4 | 0.0245381 |

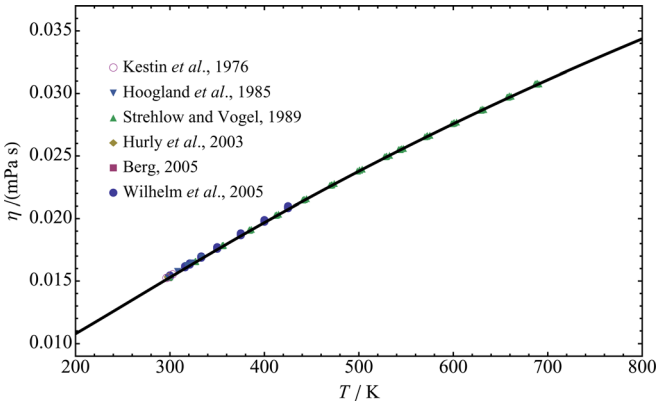


FIG. 1. (Color online) $SF_6$ dilute-gas model (solid line) along with low-density primary data.

Kestin *et al.*,[28] Hellemans *et al.*,[25] Kestin *et al.*,[43] Dawe *et al.*,[23] Raw and Tang,[22] Ellis and Raw,[21] McCoubrey and Singh,[20] and Earwicker and Fear.[19] As shown in Fig. 2, with the exception of the Ellis and Raw[21] data, all low-density gaseous data are in reasonable agreement with the dilute-gas model. Ellis and Raw[21] noted that at temperatures above 1023 K the experimental data are unreliable, due to thermal dissociation.

Figure 3 shows comparisons with some other zero-density and atmospheric-pressure formulations in the literature. The formulation of Altunin[11] is valid from 218 K to 873 K and has an estimated uncertainty of 1%; Equation (6) is in agreement with this curve to within this level of uncertainty. The "individual" correlation from Strehlow and Vogel[37] has an estimated uncertainty of about 0.3% for the temperature range from room temperature up to 700 K and is in agreement with Eq. (6) to within its estimated uncertainty. At temperatures below room temperature, the estimated uncertainty of the correlation from Strehlow and Vogel[37] (as well as our correlation) is larger due to the underlying data—the low-temperature data of Harris *et al.*[32] upon which the individual correlation was based have an estimated uncertainty of 1.5%.[37] Until additional low-temperature data of low

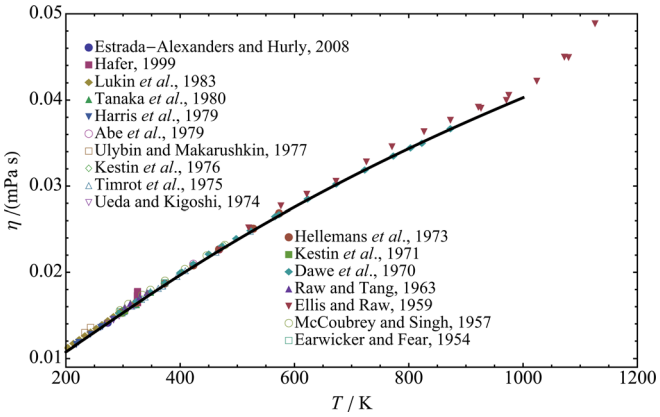


FIG. 2. (Color online) $SF_6$ dilute-gas model (solid line) along with low-density secondary and other data.

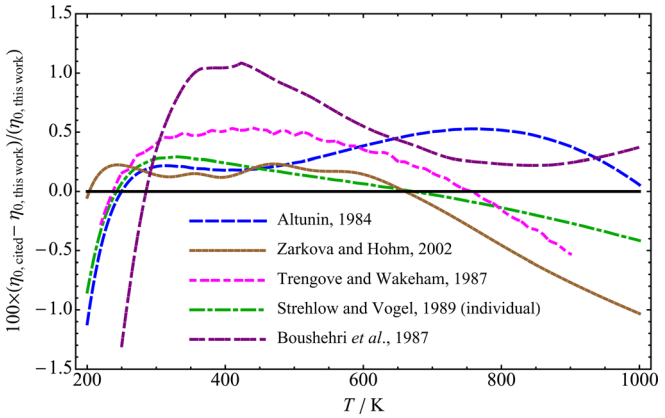


FIG. 3. (Color online) Comparison of zero-density and atmospheric-pressure correlations in the literature.

uncertainty become available, it is not possible to improve any correlation in this region. The correlation of Trengove and Wakeham[47] has an uncertainty of 0.3% at room temperature, rising to 1.5% at 220 K and 2% at 900 K, and is in agreement with Eq. (6) to within their estimated uncertainties. The formulation of Zarkova and Hohm[48] incorporated the data of Strehlow and Vogel[37] and is in good agreement with Eq. (6) and the correlation of Strehlow and Vogel[37] at low temperatures. Larger deviations are seen at high temperatures, but the agreement is still within the uncertainty of the data. Finally, Fig. 3 shows reasonable agreement with the correlation of Boushehri *et al.*,[49] claimed to be valid from 250 K to 3000 K.

### 2.2. Initial density dependence

Subsequent to the derivation of the dilute-gas-limit model, a model for the initial density dependence (second viscosity virial coefficient) of $SF_6$ was derived. This was done in order to ensure agreement with the Rainwater–Friend[50] theory. The second viscosity virial coefficient is defined as

$$B_\eta = \frac{1}{\eta_0}\left(\partial\eta \Big/ \partial p\right)_{\rho=0}. \tag{7}$$

In terms of the formulation given in Eq. (5), this reduces to

$$B_\eta = \frac{RT}{\eta_0}\kappa_i. \tag{8}$$

The $\kappa_i$ is parameterized according to the recommended form for the GFT,

$$\kappa_i = (c_0 + c_1\psi_1 + c_2\psi_2)/T_r, \tag{9}$$

where

$$\psi_1 = \exp\left(T_r^{-1}\right) - 1 \tag{10}$$

and

$$\psi_2 = \exp\left(T_r^{-2}\right) - 1. \tag{11}$$

TABLE 3. Parameters for the second viscosity virial coefficient, Eq. (9)

| $i$ | $c_i\left(\frac{\text{mPa s}}{\text{bar}}\right)$ |
|---|---|
| 0 | $5.38783 \times 10^{-5}$ |
| 1 | $1.63805 \times 10^{-6}$ |
| 2 | $-2.08160 \times 10^{-5}$ |

The fitted parameters in Eq. (9) for the second viscosity virial coefficient are reported in Table 3. Figure 4 shows a comparison between the reduced second viscosity virial coefficient calculated by the model derived in this work, and the model of Vogel *et al.*[42] using the $SF_6$ intermolecular parameters of Strehlow and Vogel[37] ($\varepsilon/k_B = 215.0$ K and $\sigma = 0.5205$ nm), along with reduced $B_\eta$ values derived from the experimental results of Strehlow and Vogel[37] and Wilhelm *et al.*[10] The reducing parameters used in Fig. 4 are the critical temperature $T_c$ and the critical volume $v_c$. The model performance is in basic agreement with the Rainwater–Friend[50] theory and shows reasonable agreement, being in the right order of magnitude with the experimental values, as shown in Fig. 4.

### 2.3. Residual friction model

The mathematical form for the temperature-dependent residual friction coefficients is essentially similar to that originally proposed.[18] The proposed temperature dependence of the friction constants is of the form,

$$\kappa_a = (a_0 + a_1\psi_1 + a_2\psi_2)/T_r, \tag{12}$$

$$\kappa_r = (b_0 + b_1\psi_1 + b_2\psi_2)/T_r, \tag{13}$$

$$\kappa_{aa} = (A_0 + A_1\psi_1 + A_2\psi_2)/T_r^3, \tag{14}$$

$$\kappa_{rr} = (B_0 + B_1\psi_1 + B_2\psi_2)/T_r^3, \tag{15}$$

$$\kappa_{ii} = (C_0 + C_1\psi_1 + C_2\psi_2)/T_r^3, \tag{16}$$

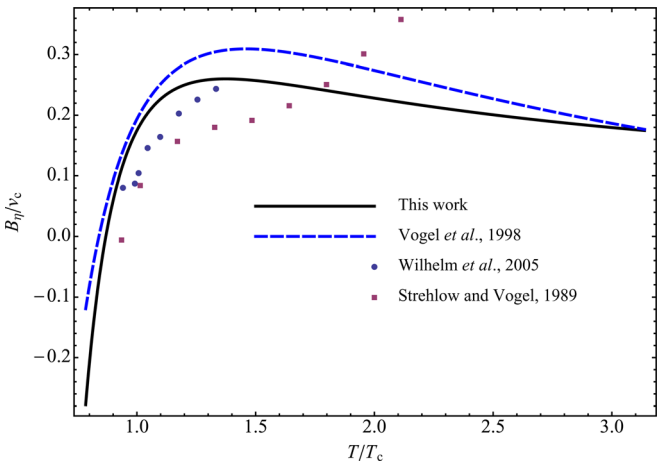


FIG. 4. (Color online) Second viscosity virial coefficient $B_\eta$.

TABLE 4. Residual friction model parameters for $SF_6$

| $i$ | $a_i$ $\left(\frac{\text{mPa s}}{\text{bar}}\right)$ | $b_i$ $\left(\frac{\text{mPa s}}{\text{bar}}\right)$ | $A_i$ $\left(\frac{\text{mPa s}}{\text{bar}^2}\right)$ | $B_i$ $\left(\frac{\text{mPa s}}{\text{bar}^2}\right)$ |
|---|---|---|---|---|
| 0 | $-6.87811 \times 10^{-4}$ | $1.72737 \times 10^{-4}$ | $9.99563 \times 10^{-8}$ | $-8.98256 \times 10^{-8}$ |
| 1 | $8.22661 \times 10^{-4}$ | $-2.02448 \times 10^{-4}$ | $-9.64167 \times 10^{-9}$ | $-8.49428 \times 10^{-8}$ |
| 2 | $-3.54867 \times 10^{-4}$ | $1.95952 \times 10^{-4}$ | $-7.54196 \times 10^{-9}$ | 0 |
| | $C_i$ $\left(\frac{\text{mPa s}}{\text{bar}^3}\right)$ | $D_i$ $\left(\frac{\text{mPa s}}{\text{bar}^3}\right)$ | $E_i$ $\left(\frac{\text{mPa s}}{\text{bar}^3}\right)$ | |
| 0 | $-8.53432 \times 10^{-6}$ | 0 | 0 | |
| 1 | $1.14404 \times 10^{-5}$ | 0 | $-5.69402 \times 10^{-11}$ | |
| 2 | $-5.65762 \times 10^{-6}$ | $2.27980 \times 10^{-11}$ | $2.92190 \times 10^{-11}$ | |

$$\kappa_{\text{rrr}} = \left(D_0 + D_1\psi_1 + D_2\psi_2\right)/T_{\text{r}}, \tag{17}$$

and

$$\kappa_{\text{aaa}} = \left(E_0 + E_1\psi_1 + E_2\psi_2\right)/T_{\text{r}}. \tag{18}$$

## 3. Regression and Results

The final model parameters are given in Table 4 where, as in Table 3, in order to facilitate the numerical implementation of the model, the reported units for the values of the parameters are distinctively given as units of viscosity for the numerator and pressure for the denominator. There are a total of five parameters for the dilute-gas correlation and 21 for the residual terms. The parameters were fitted through an iterative regression method that used all of the primary and secondary data reported in Table 1. There are two main differences between the treatments of the primary and secondary data: (1) no secondary data that overlapped with the primary data were considered and (2) the primary data were not modified in any way, whereas the considered secondary data points were smoothed through the regression process. Tertiary data were not used at all in the regression, the principal reason being that most of the data overlapped with the primary data, which were considered to be of higher accuracy.

All of the regressions were iteratively made through a process that consisted of (1) performing a regression, (2) locating the point of highest deviation (excluding primary data), (3) if the highest deviation point was above a given tolerance, the point was smoothed by replacing it with the average between the point itself and the value predicted with the correlation. This smoothing process was iterated until a tolerance for the highest deviation of 0.5% was achieved.

The final behavior of the model is depicted in Figs. 5 and 6, showing a smooth uniform viscosity surface. In the original GFT work,[18] it was demonstrated that the GFT approach allows for the physics present in the EoS to be mapped onto the viscosity surface. In the original GFT work, $CO_2$ and water were used to illustrate the difference in the physics that results from the internal-pressure-based attraction-repulsion balance. In the case of $CO_2$, a clear attraction-repulsion separation is derived, while in the case of water at low temperature an inversion in the sign of the internal pressure develops. This anomalous behavior, in the case of water, was then linked to the low-temperature viscosity anomaly that water develops at high pressure.[18] In the case of $SF_6$, the internal pressure calculations that follow from the Guder and Wagner[8] EoS show no anomalous behavior, resulting, as

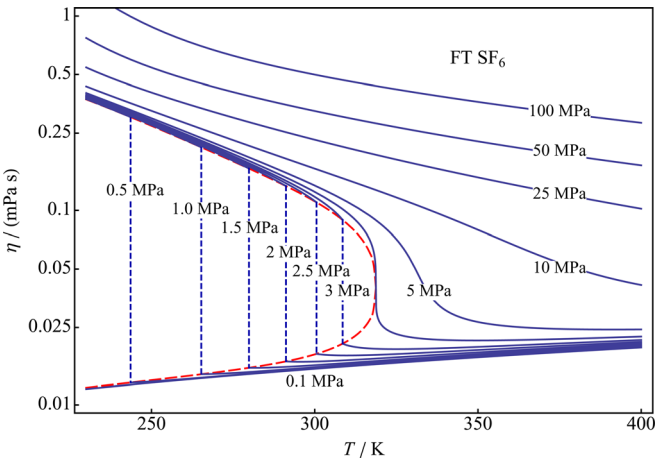


FIG. 5. (Color online) $SF_6$ model $\eta$-$T$ surface performance near the phase boundary.

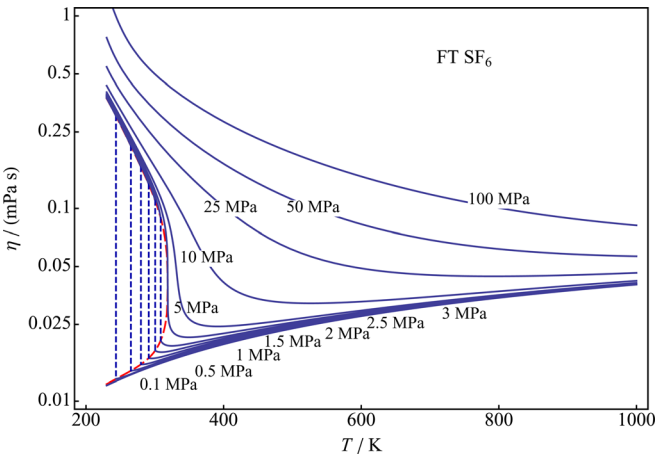


FIG. 6. (Color online) Overall $SF_6$ model $\eta$-$T$ surface performance.

depicted in Fig. 7, in a clear attraction-repulsion separation similar to the one reported in the case of $CO_2$.[18] It can therefore be argued that the regular behavior shown in Figs. 5 and 6 follows from the regular behavior that the Guder and Wagner[8] EoS shows for the $SF_6$ internal-pressure-based attraction-repulsion separation.

Table 5 shows the deviation results for the $SF_6$ primary data,[10,15,37–40,43] where the AAD, Bias, and root-mean-square error (RMS) values are defined as follows:

$$\mathrm{AAD} = 100 \times \frac{1}{n}\sum_{i=1}^{n}\left|\frac{\eta_{i,\,\mathrm{calculated}} - \eta_{i,\,\mathrm{experimental}}}{\eta_{i,\,\mathrm{experimental}}}\right|, \quad (19)$$

$$\mathrm{Bias} = 100 \times \frac{1}{n}\sum_{i=1}^{n}\left(\frac{\eta_{i,\,\mathrm{calculated}} - \eta_{i,\,\mathrm{experimental}}}{\eta_{i,\,\mathrm{experimental}}}\right), \quad (20)$$

$$\mathrm{RMS} = 100 \times \left[\frac{1}{n}\left(\sum_{i=1}^{n}\left(\frac{\eta_{i,\,\mathrm{calculated}} - \eta_{i,\,\mathrm{experimental}}}{\eta_{i,\,\mathrm{experimental}}}\right)^2\right)\right]^{1/2}. \quad (21)$$

Most of the primary data are reproduced within the uncertainty reported by the authors and cover pressure and temperature ranges in the area of industrial application. In the case of the secondary data,[12–14,21,26,31,34,36,41] Table 6 appears to

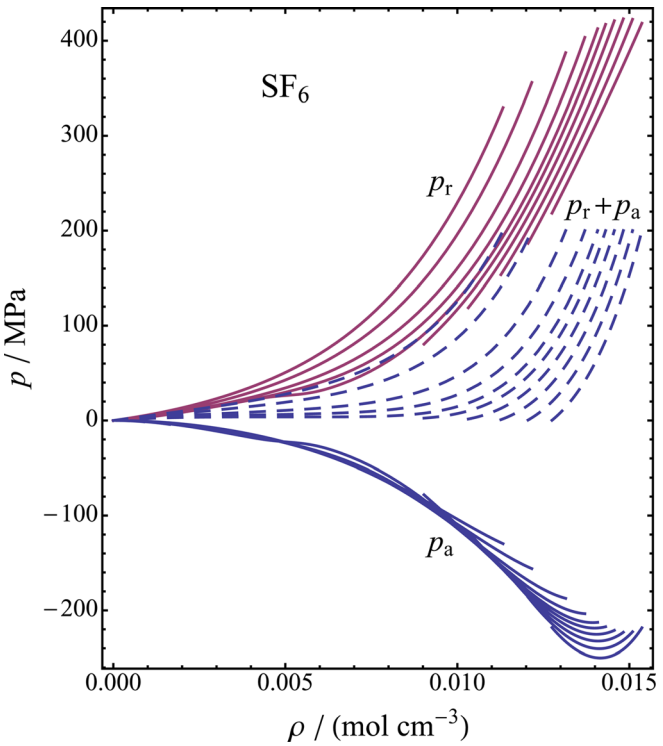


FIG. 7. (Color online) Separation of the pressure into attractive and repulsive parts based on the internal pressure Eqs. (2) and (3) for the $SF_6$ reference EoS of Guder (Ref. 8). Only stable branches are depicted at 220 K, 240 K, 260 K, 280 K, 300 K, $T_c$, 350 K, 400 K, 500 K, and 600 K.

TABLE 5. Primary data friction theory model results

| Author | $T$-range (K) | $p$-range (MPa) | Auth. Unc. (%) | AAD (%) | Bias (%) | RMS (%) | $n$ |
|---|---|---|---|---|---|---|---|
| Kestin *et al.*[43] | 296–303 | 0.1 | 0.1 | 0.27 | −0.27 | 0.27 | 2 |
| Hoogland *et al.*[15] | 298–333 | 0.1–9.6 | 0.10 | 0.29 | −0.28 | 0.34 | 31 |
| Strehlow and Vogel[37] | 299–691 | 0–0.3 | 0.1–0.3 | 0.09 | 0.02 | 0.10 | 77 |
| Hurly *et al.*[38] | 298–298 | 0.3–1.6 | 0.50 | 0.17 | 0.12 | 0.19 | 15 |
| Wilhelm *et al.*[10] | 300–425 | 0–20.4 | 0.25 | 0.20 | −0.02 | 0.29 | 677 |
| Berg[39,40] | 298–298 | 0.1 | 0.04 | 0.04 | −0.04 | 0.04 | 1 |

TABLE 6. Secondary data friction theory model results

| Author | $T$-range (K) | $p$-range (MPa) | Auth. Unc. (%) | AAD (%) | Bias (%) | RMS (%) | $n$ |
|---|---|---|---|---|---|---|---|
| Ellis and Raw[21] | 470–1126 | 0.1 | 1.00 | 3.05 | −2.99 | 3.81 | 17 |
| Ueda and Kigoshi[26] | 273–346 | 0.1 | 4.00 | 0.70 | 0.58 | 0.77 | 8 |
| Timrot *et al.*[13] | 297–526 | 0–3.5 | 0.7 | 0.58 | −0.48 | 1.00 | 62 |
| Ulybin and Makarushkin[12,a] | 230–318 | 3–51.2 | 1.00 | 1.39 | 0.56 | 2.88 | 85 |
| Grigorev *et al.*[14] | 245–473 | 2–40 | 0.7–1.1 | 2.33 | −0.88 | 4.49 | 131 |
| Abe *et al.*[31] | 423–468 | 0.1 | 0.30 | 0.55 | −0.55 | 0.70 | 2 |
| Hoogland and Trappeniers[34,b] | 319–323 | 3.8–4.1 | 0.1–1 | 6.92 | −6.92 | 8.70 | 13 |
| Takahashi *et al.*[36,c] | 273–319 | 1.2–3.7 | 0.50 | 1.56 | 1.54 | 1.96 | 34 |
| Estrada-Alexanders and Hurly[41] | 273–273 | 0.3–1.0 | 0.60 | 1.65 | 0.06 | 2.57 | 8 |

[a]Includes sat. liquid, sat. vapor, excluding critical region points.
[b]Critical isochore.
[c]Saturated vapor.

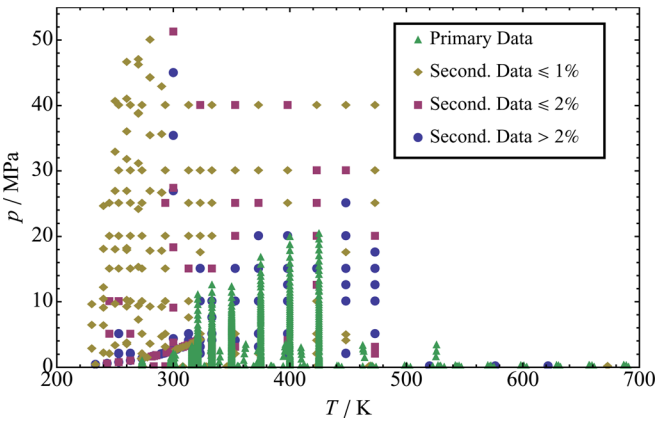


FIG. 8. (Color online) Deviation-$p$-$T$ diagram.

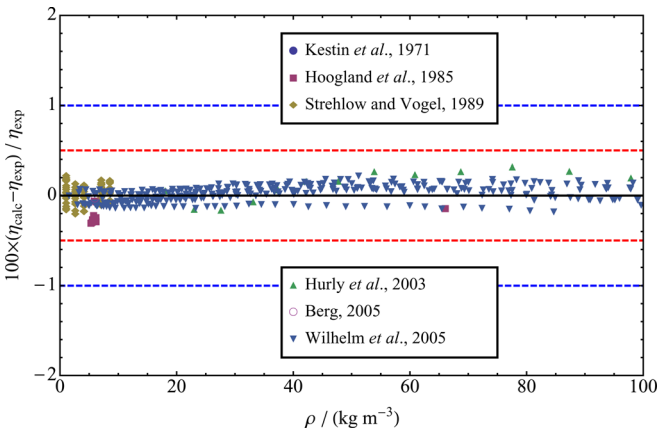


FIG. 9. (Color online) Low-density primary data model deviation. Calculated value: $\eta_{calc}$, experimental value: $\eta_{exp}$.

show larger overall discrepancies. However, more illustrative are the results shown in the deviation diagram presented in Fig. 8. This deviation diagram shows that for the main region of application covering a temperature range between 250 K and 500 K and pressures up to 50 MPa, the model also reproduces most of the secondary data within 1%. In fact, the largest deviations related to the secondary data are mostly found in the region of overlap with the primary data, i.e., a region where only primary data were considered in the regression. The primary data have overall deviations under 0.5%. For the high-temperature region, high-pressure data are unavailable. Nevertheless, the core of the GFT model is the Guder–Wagner EoS, and therefore, following Guder and Wagner,[8] we expect that the viscosity model can also be extrapolated with physically reasonable behavior to high temperatures and pressures beyond the range of data availability used in the regression of the EoS (triple point to 625 K and up to 150 MPa). This is further supported by the smooth and regular behavior shown in Figs. 5 and 6.

Table 7 reports the model deviation results for the tertiary data.[16,19,20,22,23,25,28–30,32,33,35] As shown in the table, most of the data are reproduced within or close to the reported uncertainty. It should be noted that the main reason that most of the tertiary data were not considered was simply because of their overlap with the primary data.

### 3.1. Low-density results

Figures 9 and 10 show the percentage deviations of the low-density (less than 100 kg m$^{-3}$) primary and secondary data. The temperature range for the low-density data can be seen in Figs. 1 and 2. The deviation values in these figures can be considered to be controlled mainly by the dilute-gas limit model. Therefore, based on comparisons with data, the dilute-gas model is estimated to have an uncertainty of 0.3% (at a coverage factor of two) for the temperature range 298 K to 700 K, rising to 1.5% at both the lowest (the triple point) and highest (1000 K) values of its recommended temperature range.

### 3.2. Full-range results

Figures 11–13 show the FT model viscosity deviation trends with density, pressure, and temperature with respect

TABLE 7. Tertiary data friction theory model results

| Author | $T$-range (K) | $p$-range (MPa) | Auth. Unc. (%) | AAD (%) | Bias (%) | RMS (%) | $n$ |
|---|---|---|---|---|---|---|---|
| Earwicker and Fear[19] | 296–373 | 0.1 | n/a | 1.27 | −1.27 | 1.35 | 2 |
| McCoubrey and Singh[20] | 295–478 | 0.1 | 1 | 1.90 | −0.47 | 2.08 | 8 |
| Raw and Tang[22] | 303–342 | 0 | 1.00 | 2.77 | −2.77 | 2.78 | 4 |
| Dawe *et al.*[23] | 293–873 | 0.1 | 1.00 | 0.55 | −0.40 | 0.67 | 20 |
| Hellemans *et al.*[25] | 298–573 | 0.1 | 0.1–0.3 | 0.34 | −0.34 | 0.36 | 7 |
| Kestin *et al.*[28] | 296–477 | 0.1 | 0.2 | 0.46 | −0.46 | 0.48 | 3 |
| Kestin *et al.*[29] | 296–474 | 0.1 | 0.1–0.2 | 0.38 | −0.38 | 0.44 | 10 |
| Kestin *et al.*[30] | 298–473 | 0.1 | 0.1–0.2 | 0.29 | −0.29 | 0.33 | 5 |
| Harris *et al.*[32] | 218–302 | 1 | 1.00 | 0.22 | 0.05 | 0.26 | 7 |
| Tanaka *et al.*[33] | 298–348 | 0.1–0.2 | 1.00 | 0.71 | −0.10 | 0.80 | 12 |
| Lukin *et al.*[35,a] | 173–293 | 0.1 | 0.30 | 1.91 | −1.91 | 1.94 | 7 |
| Hafer[16,b] (forced mode) | 225–326 | 0.07–34.5 | 3–6 | 3.26 | −2.00 | 4.09 | 1108 |
| Hafer[16,b] (free mode) | 226–327 | 0.03–4.46 | 3–6 | 3.64 | −3.19 | 4.67 | 967 |

[a]Excludes points below triple point.
[b]Includes liquid, vapor, and supercritical states.

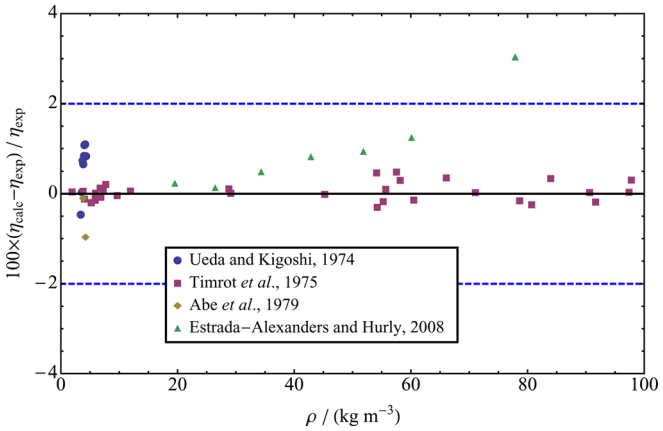


FIG. 10. (Color online) Low-density secondary data model deviations. Calculated value: $\eta_{calc}$, experimental value: $\eta_{exp}$.

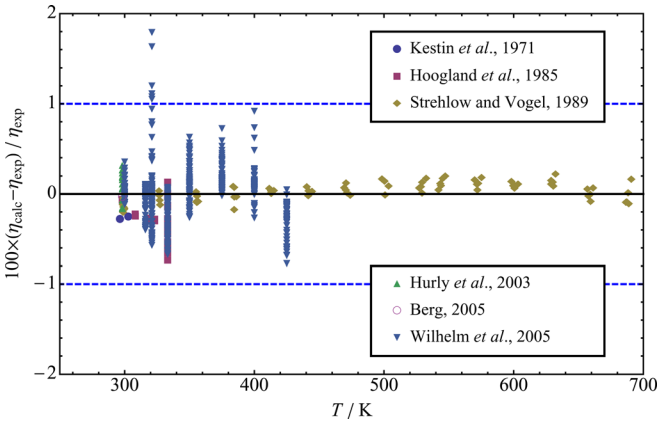


FIG. 13. (Color online) Full temperature range primary data model deviations. Calculated value: $\eta_{calc}$, experimental value: $\eta_{exp}$.

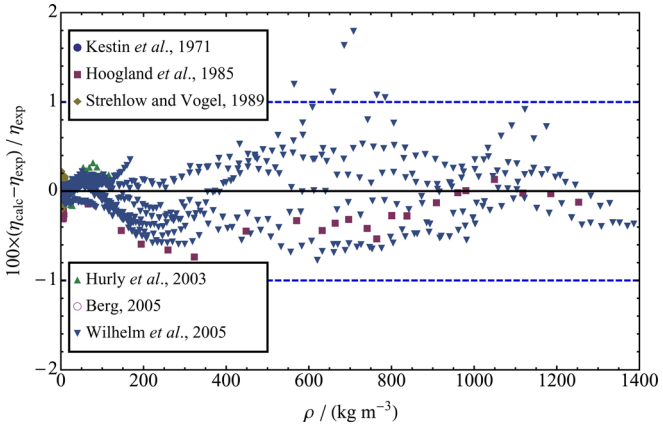


FIG. 11. (Color online) Full density range primary data model deviations. Calculated value: $\eta_{calc}$, experimental value: $\eta_{exp}$.

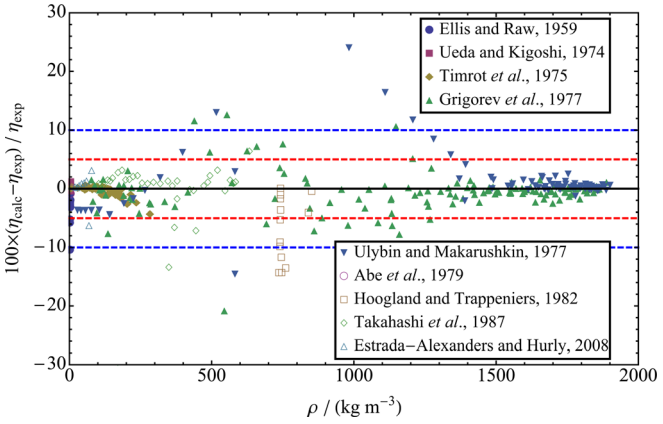


FIG. 14. (Color online) Full density range secondary data model deviations. Calculated value: $\eta_{calc}$, experimental value: $\eta_{exp}$.

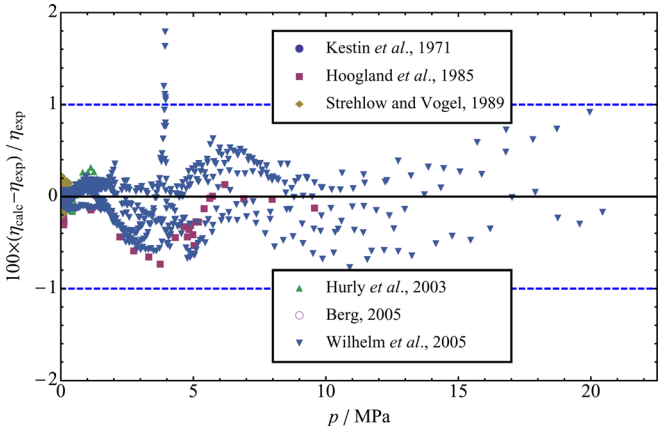


FIG. 12. (Color online) Full pressure range primary data model deviations. Calculated value: $\eta_{calc}$, experimental value: $\eta_{exp}$.

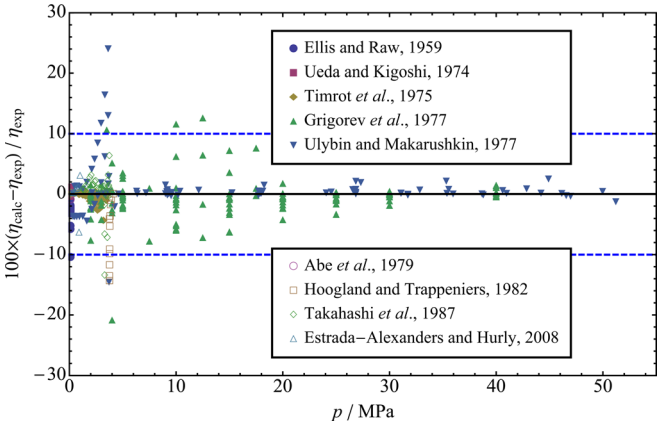


FIG. 15. (Color online) Full pressure range secondary data model deviations. Calculated value: $\eta_{calc}$, experimental value: $\eta_{exp}$.

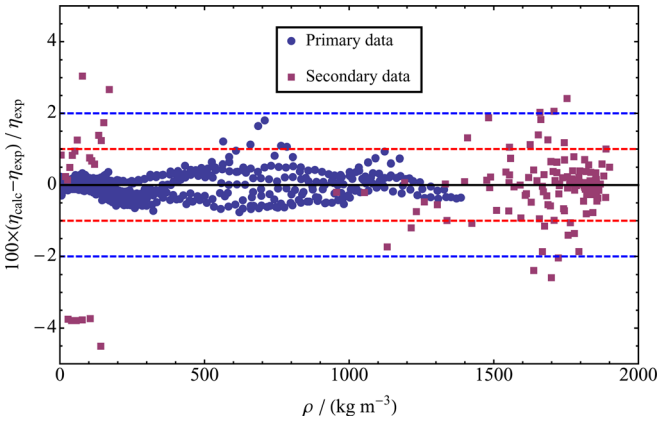


FIG. 16. (Color online) Overall deviation performance of all data considered in the regression.

to the primary data. The largest deviation is observed near the critical point which is located at 742.3 kg $m^{-3}$, 3.755 MPa, and 318.7 K. Figures 14 and 15 show the FT model pressure deviation trends for the secondary data showing a good high-pressure/density trend. The deviations shown are computed with the full original data sets, not the reduced secondary data (after eliminating the points overlapping with the primary data) used in the regression process. Figures 14 and 15 report the full sets of secondary data. Figure 16, on the other hand, shows the combined primary and secondary data deviations, from the triple point to 700 K, but eliminating the secondary data that overlap with the primary data, i.e., eliminating the non-considered secondary data. Figure 16 shows the full-range model performance. It should be noted that the data points that fall outside the ±2% band correspond to data points below 300 K. Also, Fig. 16 is presented in a density range up to 2000 kg $m^{-3}$, which is higher than the maximum density for 100 MPa and temperatures above 300 K (1920 kg $m^{-3}$ at 300 K). Overall, considering both the primary and secondary performance, outside the critical region, the model delivers reasonable unbiased high-pressure as well as high-temperature trends in relation to the considered data. As depicted in Fig. 16, the density trends above 300 K are mostly confined within the ±1% bandwidth, and therefore it would be reasonable to assume that, for temperatures above 300 K and densities below 2000 kg $m^{-3}$ (conditions up to 100 MPa), the expected model performance should fall within the ±2% bandwidth, i.e., an uncertainty of approximately 2%–3% for extrapolations up to 100 MPa above 300 K.

TABLE 8. Sample points for computer verification of the model

| Temperature (K) | Density (kg $m^{-3}$) | Viscosity (μPa s) |
|---|---|---|
| 300 | 0 | 15.2887 |
| 300 | 5.92 | 15.3043 |
| 300 | 1345.1 | 117.417 |
| 400 | 0 | 19.6796 |
| 400 | 278.47 | 24.4272 |
| 400 | 1123.8 | 84.7835 |

## 4. Computer-Program Verification

Table 8 is provided to assist in computer-program verification. The viscosity calculations are based on the tabulated temperatures and densities.

## 5. Conclusion

We have developed, based on GFT and available experimental data, a wide-ranging model for the viscosity surface of $SF_6$ that is valid from the triple point to 1000 K. It has been validated with experimental data up to 50 MPa, and extrapolates in a physically reasonable manner up to 100 MPa. The formulation has been developed with the EoS of Guder and Wagner,[8] and provides a viscosity surface for $SF_6$ valid over the entire fluid region including liquid, gas and supercritical states.

The correlation reproduces most of the primary data close to or within the reported uncertainty (0.1%–0.5%). It performs best in the low-pressure (less than 0.33 MPa) region from 300 K to 700 K where the estimated uncertainty (considered to be combined expanded uncertainty with a coverage factor of two) is 0.3%. In the region from 300 K to 425 K for pressures less than 20 MPa, corresponding to the region measured by Wilhelm *et al.*,[10] the estimated uncertainty is less than 1%. Where there were data available for validation at temperatures from 230 K to 575 K for pressures up to 50 MPa, the estimated uncertainty is 2%.

## Acknowledgments

We thank Dr. Arno Laesecke (NIST), Professor Christian Boned (University of Pau, France), and Professor Marc Assael (Aristotle University, Greece) for helpful suggestions.

## 6. References

[1]L. G. Christophorou and R. J. Vanbrunt, IEEE Trans. Diel. Electr. Insul. **2**, 952 (1995).
[2]E. C. Ihmels and J. Gmehling, Int. J. Thermophys. **23**, 709 (2002).
[3]Y. Z. Zhao, Y. K. Luo, Y. Zhang, X. G. Mei, and J. Tang, Ultrasound Med. Biol. **31**, 537 (2005).
[4]F. Höhn, A. Mirshahi, and L. O. Hattenbach, Ophthalmologe **107**, 328 (2010).
[5]A. Olivet and L. F. Vega, J. Chem. Phys. **126**, 144502 (2007).
[6]G. S. Pawley, Mol. Phys. **43**, 1321 (1981).
[7]D. Dellis and J. Samios, Fluid Phase Equilib. **291**, 81 (2010).
[8]C. Guder and W. Wagner, J. Phys. Chem. Ref. Data **38**, 33 (2009).
[9]M. J. Assael, I. A. Koini, K. D. Antoniadis, M. L. Huber, I. M. Abdulagatov, and R. A. Perkins, "Reference Correlation of the Thermal Conductivity of Sulfur Hexafluoride from the Triple Point to 1000 K and up to 150 MPa" J. Phys. Chem. Ref. Data (in press).
[10]J. Wilhelm, D. Seibt, E. Bich, E. Vogel, and E. Hassel, J. Chem. Eng. Data **50**, 896 (2005).
[11]V. V. Altunin, Tr. Mosk. Energy Inst. **622**, 12 (1984).
[12]S. A. Ulybin and V. I. Makarushkin, High Temp. **15**, 1022 (1977).
[13]D. L. Timrot, M. A. Serednitskaya, and S. A. Traktueva, High Temp. **13**, 1031 (1975).
[14]V. A. Grigorev, A. S. Keramidi, V. K. Grachev, and Y. L. Rastorguev, Therm. Eng. **24**, 66 (1977).
[15]J. H. B. Hoogland, H. R. Vandenberg, and N. J. Trappeniers, Physica A **134**, 169 (1985).
[16]R. F. Hafer, MS thesis, University of Colorado, 1999.
[17]R. F. Hafer and A. Laesecke, Meas. Sci. Technol. **14** (2003).

[18]S. E. Quiñones-Cisneros and U. K. Deiters, J. Phys. Chem. B **110**, 12820 (2006).
[19]G. A. Earwicker and E. J. P. Fear, Chem. Ind. (London), **29**, 903 (1954).
[20]J. C. McCoubrey and N. M. Singh, Trans. Farad. Soc. **53**, 877 (1957).
[21]C. P. Ellis and C. J. G. Raw, J. Chem. Phys. **30**, 574 (1959).
[22]C. J. G. Raw and H. Tang, J. Chem. Phys. **39**, 2616 (1963).
[23]R. A. Dawe, G. C. Maitland, M. Rigby, and E. B. Smith, Trans. Farad. Soc. **66**, 1955 (1970).
[24]J. Kestin, E. Paykoç, and J. V. Sengers, Physica **54**, 1 (1971).
[25]J. M. Hellemans, J. Kestin, and S. T. Ro, Physica **65**, 376 (1973).
[26]K. Ueda and K. Kigoshi, J. Inorg. Nucl. Chem. **36**, 989 (1974).
[27]D. L. Timrot and S. A. Traktueva, Therm. Eng. **22**, 105 (1975).
[28]J. Kestin, H. E. Khalifa, and W. A. Wakeham, J. Chem. Phys. **65**, 5186 (1976).
[29]J. Kestin, H. E. Khalifa, S. T. Ro, and W. A. Wakeham, Physica **88A**, 242 (1977).
[30]J. Kestin, H. E. Khalifa, and W. A. Wakeham, J. Chem. Phys. **67**, 4254 (1977).
[31]Y. Abe, J. Kestin, H. E. Khalifa, and W. A. Wakeham, Ber. Bunsenges. Phys. Chem. **83**, 271 (1979).
[32]E. J. Harris, G. C. Hope, D. W. Gough, and E. B. Smith, J. Chem. Soc., Faraday Trans. 1 **75**, 892 (1979).
[33]Y. Tanaka, M. Nakajima, H. Kubota, and T. Makita, J. Chem. Eng. Jpn. **13**, 155 (1980).
[34]J. H. B. Hoogland and N. J. Trappeniers, in *Proceedings 8th Symposium on Thermophysical Properties*, edited by J. V. Sengers (American Society of Mechanical Engineers, New York, 1982), p. 440.
[35]V. I. Lukin, B. A. Ivakin, and P. E. Suetin, Zh. Tekh. Fiz. **53**, 931 (1983).
[36]M. Takahashi, C. Yokoyama, and S. Takahashi, in *Proceedings of the Eighth Japan Symposium on Thermophysical Properties* (Japanese Thermophysical Properties Society, Tokyo, 1987), p. 125.
[37]T. Strehlow and E. Vogel, Physica A **161**, 101 (1989).
[38]J. J. Hurly, K. A. Gillis, J. B. Mehl, and M. R. Moldover, Int. J. Thermophys. **24**, 1441 (2003).
[39]R. F. Berg, Metrologia **42**, 11 (2005).
[40]R. F. Berg, Metrologia **43**, 183 (2006).
[41]A. F. Estrada-Alexanders and J. J. Hurly, J. Chem. Thermodyn. **40**, 193 (2008).
[42]E. Vogel, C. Küchenmeister, E. Bich, and A. Laesecke, J. Phys. Chem. Ref. Data **27**, 947 (1998).
[43]J. Kestin, S. T. Ro, and W. A. Wakeham, Trans. Farad. Soc. **67**, 2308 (1971).
[44]H. Preston-Thomas, Metrologia **27**, 3 (1990).
[45]J. V. Sengers, R. A. Perkins, M. L. Huber, and D. G. Friend, Int. J. Thermophys. **30**, 374 (2009).
[46]M. Funke, R. Kleinrahm, and W. Wagner, J. Chem. Thermodyn. **34**, 735 (2002).
[47]R. D. Trengove and W. A. Wakeham, J. Phys. Chem. Ref. Data **16**, 175 (1987).
[48]L. Zarkova and U. Hohm, J. Phys. Chem. Ref. Data **31**, 183 (2002).
[49]A. Boushehri, J. Bzowski, J. Kestin, and E. A. Mason, J. Phys. Chem. Ref. Data **16**, 445 (1987).
[50]J. C. Rainwater and D. G. Friend, Phys. Rev. A **36**, 4062 (1987).